THE JOURNAL OF PHYSICAL CHEMISTRY C

Article

pubs.acs.org/JPCC

Interaction of Probe Molecules with Bridging Hydroxyls of Two-Dimensional Zeolites: A Surface Science Approach

J. Anibal Boscoboinik,*[,†] Xin Yu,[†] Emre Emmez,[†] Bing Yang,[†] Shamil Shaikhutdinov,[†] Frank D. Fischer,[‡] Joachim Sauer,*[,‡] and Hans-Joachim Freund[†]

[†]Fritz-Haber-Institut der Max-Planck-Gesellschaft, Faradayweg 4 - 6, 14195 Berlin, Germany

[‡]Humboldt-Universität zu Berlin, Department of Chemistry, Unter den Linden 6, 10009 Berlin, Germany

Supporting Information

ABSTRACT: Bridging hydroxyls (Si−OH−Al) in zeolites are catalytically active for a multitude of important reactions, including the catalytic cracking of crude oil, oligomerization of olefins, conversion of methanol to hydrocarbons, and the selective catalytic reduction of NO_x. The interaction of probe molecules with bridging hydroxyls was studied here on a novel two-dimensional zeolite model system consisting of an aluminosilicate forming a planar sheet of polygonal prisms, supported on a Ru(0001) surface. These bridging hydroxyls are strong Brönsted acid sites and can interact with both weak and strong bases. This interaction is studied here for two weak bases (CO and C_2H_4) and two strong bases (NH_3 and pyridine), by infrared reflection absorption spectroscopy, in comparison with density functional theory calculations. Additionally, ethene is the reactant in the simplest case of the olefin oligomerization reaction which is also catalyzed by bridging hydroxyls, making the study of this adsorbed precursor state particularly relevant. It is found that weak bases interact weakly with the proton without breaking the O−H bond, although they do strongly affect the O−H stretching vibration. On the other hand, the strong bases, NH_3 and pyridine, abstract the proton to produce ammonium and pyridinium ions. The comparison with the properties of three-dimensional zeolites shows that this two-dimensional zeolite model system counts with bridging hydroxyls with properties similar to those of the most catalytically active zeolites, and it provides critical tools to achieve a deeper understanding of structure−reactivity relations in zeolites.

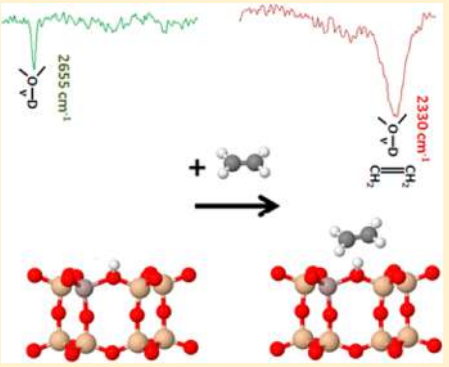

1. INTRODUCTION

Zeolites are ordered porous materials composed of a network of $SiO_{4/2}$ and $AlO_{4/2}^-$ tetrahedra, and they are used in a wide variety of technological and industrial applications.[1] In particular, the impact they have in heterogeneous catalysis makes these materials one of the most important ones in the field.[2] They are widely used as solid catalysts, in reactions such as the catalytic cracking of crude oil, methanol to gasoline conversion, oligomerization of olefins, and the selective catalytic reduction of NO_x, among many others. The presence of acidic hydroxyl groups within the pores plays a crucial role in their catalytic activity. Particularly, bridging hydroxyls, i.e., those arising from the protonation of an oxygen atom bridging Si and Al, can have an acidic strength approaching that of superacids.[3] These have been extensively studied by experimental and theoretical methods.[3−5]

While surface science has been able to provide mechanistic details of reactions on many metallic and oxide catalysts,[6] the preparation of a model system for zeolites was previously regarded as an impossible task.[7]

In a recent letter we described the preparation of an ultrathin aluminosilicate system presenting the required features to model zeolites from a surface science approach.[8] Although other ring sizes were found in the framework,[9] the majority of the film comprises a two-dimensional arrangement of hexagonal prisms, and we will therefore call this film 2dH (2-dimensional Hexagonal) in this manuscript. The protonated and deuterated forms will be referred to as H-2dH and D-2dH, respectively. One of the ways to characterize bridging hydroxyls is by adsorption of probe molecules.[3,10] Note that our silica bilayer does not have dangling bonds saturated by surface hydroxyls as external surfaces of zeolites or mesoporous materials have. They are genuine models of the internal surface of zeolites representing infinitely large pores. This opens new possibilities for studying phenomena that depend on pore size such as surface curvature effects on adsorption energy.[11] Nicholas and Haw found experimentally that the proton transfer to form a carbenium ion depends on the proton affinity of the parent hydrocarbon.[12] A generalization of this was found later, by theoretical methods, such that any molecule with a proton affinity close to that of ammonia (854 kJ/mol) or larger gets protonated upon interaction with the bridging hydroxyl, while molecules with lower proton affinity (weaker bases) form a H-bonded complex.[13,14]

In our previous report,[8] the presence of bridging hydroxyls in H(D)-2dH was demonstrated by adsorption of carbon monoxide as a probe molecule, which forms an adduct with

Received: June 8, 2013
Published: June 10, 2013

   dx.doi.org/10.1021/jp405533s | J. Phys. Chem. C 2013, 117, 13547−13556

the proton and induces a red shift of the O−H stretching vibration, with the magnitude of the shift being proportional to the acidity. The results were found to be comparable to zeolite H−CHA, which is also composed of hexagonal prisms but in a three-dimensional arrangement. Other probes are also used for zeolites to determine the presence of acidic sites within the pores of the framework.[3] The present manuscript, in addition to CO, reports infrared spectra of this film after reaction with probe molecules C_2H_4, NH_3, and pyridine (Py). Similar to CO, ethene is a weak base, and it can also be used as a probe molecule to gauge the strength of the acid site, based on the shift induced on the OH vibrational frequency. It has been shown, indeed, that the shifts induced by CO and ethene are directly proportional to each other for OH groups in different materials.[15] More importantly, ethene, the simplest olefin, is the reactant in the ethene oligomerization reaction which is also catalyzed by bridging hydroxyls, and thus the use of this probe molecule provides information about the precursor state for this reaction.[16] Until now, much of the details about the adsorption geometry of such probe molecules (and reactants) came from theoretical models based on educated assumptions.[17] By using a well-defined model system and the analytical tools of surface science,[8,9] experimental data can provide a more detailed understanding of the interaction of different molecules with the active sites on zeolites and ultimately give insights about precursor states and reaction mechanisms. Additionally, the study of the behavior of probe molecules on the aluminosilicate film, in comparison with the real zeolite catalysts, allows the validation of the use of this model system for mechanistic studies of some of the most important reactions in the industry.

2. EXPERIMENTAL METHODS

The sample preparation and experiments reported here were performed in an ultrahigh-vacuum system counting with the following techniques: low-energy electron diffraction (LEED), X-ray photoelectron spectroscopy (XPS), infrared reflection absorption spectroscopy (IRAS), and scanning tunneling microscopy (STM). The Ru(0001) surface was cleaned with cycles of argon ion sputtering and annealing to ∼1200 °C. The clean surface was then precovered with a 3O-(2 × 2) overlayer by exposing to 3×10^{-6} mbar O_2 at 950 °C. Then ∼0.66 ML (1 ML = 1.57×10^{15} atoms/cm^2) of Si and ∼0.34 ML of Al were subsequently deposited onto the surface under an O_2 pressure of 2×10^{-7} mbar while the sample was kept at 100 K. At this step, partially oxidized Si and Al were determined by XPS. The film was then oxidized by exposing it to a pressure of O_2 of 3×10^{-6} mbar while heating the sample up to ∼1200 K, keeping it at this temperature for 10 min and then slowly cooling it always under an O_2 ambient. The characterization of the prepared film by XPS, IRAS, STM, and LEED is included in the Supporting Information. Hydroxylation was done by adsorbing multilayer amounts of H_2O or D_2O at 100 K and subsequently heating to temperatures above 300 K to desorb the multilayer, resulting in the characteristic frequencies for the bridging OH (OD) vibration at ∼3594 cm^{-1} (∼2654 cm^{-1}) as measured by IRAS. All spectra are shown in transmittance mode. Probe molecules (ammonia, pyridine, CO, or ethene) were dosed on the surface and their geometry and interaction with the bridging OH (OD) studied by IRAS. For ammonia and pyridine adsorption the sample was kept at 300 K to prevent the condensation of multilayer, while for C_2H_4 and CO the sample was kept at ∼100 K. For the case of CO, the spectrum was taken with the sample under a CO pressure of 2×10^{-5} mbar CO.

3. COMPUTATIONAL METHODS

All calculations were based on density functional theory with periodic boundary conditions and carried out using the Vienna ab initio simulation package (VASP), along with the projector augmented wave (PAW) method. We apply the PBE functional, augmented with a semiempirical $1/r^6$ dispersion term (PBE+D). All calculations were carried out at the Γ-point, using a plane-wave cutoff energy of 600 eV.

If not explicitly stated otherwise, the following cell parameters were used: For the calculations on the bilayer, the $AlSi_7O_{16}H$ unit cell (a = 539.61, b = 934.64, c = 2700.0 pm, $\alpha = \beta = \gamma = 90°$) used previously[8] was doubled along its shortest axis, resulting in a 1079.2 × 934.64 × 2700.0 pm cell. One and two molecules were adsorbed per double cell. For chabasite, the cell parameters were optimized for a $(HAlSi_{11}O_{24})_2$ double cell (a = 942.63 pm, b = 937.16 pm, c = 1870.80 pm, α = 93.530°, β = 94.120°, γ = 94.491°). Molecules in the gas phase were calculated using a box with the same cell parameters as in the adsorbed state.

The positions of the nuclei were relaxed until the forces were smaller than 0.05 eV/Å. Harmonic vibrational frequencies were calculated using a central finite difference method with 0.015 Å displacements in each Cartesian direction. In the case of CO adsorption, vibrational frequencies for OH and CO stretching modes were calculated from the PBE+D bond distances, making use of the ω/r correlation and anharmonicity corrections proposed by Nachtigall for CO adsorption on H/Ferrierite.[18] The vibrational frequencies reported along the text correspond to the case of one molecule adsorbed per double cell.

4. RESULTS AND DISCUSION

The side view of the structure of H-2dH is schematically shown in Figure 1, where one of the bridging hydroxyl groups is

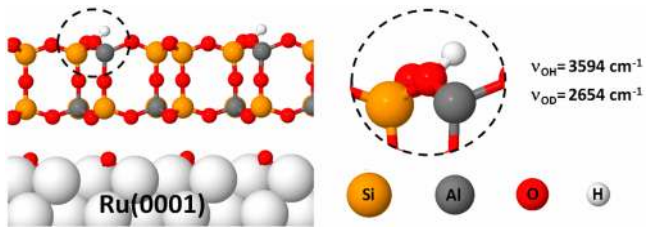

Figure 1. Structure of the bilayer aluminosilicate film exposing a bridging hydroxyl (Si−OH−Al) group.

emphasized by a dashed circle. The film has the composition $Al_xSi_{(1-x)}O_2^{x-}$, where at least some of the negative charge has been compensated by protonation of the bridging oxygen atoms, resulting in the formation of bridging hydroxyls. It was found that bridging hydroxyls are present on the surface only when x > 0.25. The presence of bridging hydroxyls on the surface is characterized by the OH (OD) stretching vibration at ∼3594 cm^{-1} (∼2654 cm^{-1}).[8] Two differences are worth noting between the experimental system and the model that was used for the DFT(+D) calculations. First, under the assumption that the interaction with the Ru(0001) substrate is weak, the calculations are performed for a free-standing two-dimensional framework. Second, while the experiments are carried out on a

dx.doi.org/10.1021/jp405533s | J. Phys. Chem. C 2013, 117, 13547−13556

system with a ratio Si/Al ~ 2, the calculations used a ratio Si/Al = 7. This choice was made for simplicity and for comparison with the zeolite chabasite, for which Si/Al = 11 is a realistic ratio. A separate study on the effect of the Si/Al ratio is underway.

The ultimate goal of the preparation and characterization of bridging hydroxyls in H-2dH is to mimic the properties of those present in real zeolites. It is therefore useful to compare the chemical properties of these bridging hydroxyls with those of catalytically active zeolites. There are ten different framework types found in the "Database of Zeolite Structures" that have the hexagonal prism as a secondary building unit (SBU); i.e., they can be built entirely by just using hexagonal prisms, which makes them convenient candidates for comparison with H-2dH since the latter has the same SBU. These are AEI, CHA, SAV, AFT, AFX, GME, KFI, TSC, EMT, and FAU.[19] Among these, perhaps the most common ones are CHA and FAU. We will make a comparison along the manuscript with two zeolites having these framework types for which experimental data are available in the literature, namely, H-SSZ-13 (CHA) and H-Y-Zeolite (FAU). Sierka and Sauer provided a useful correlation of bridging hydroxyls, and proton jumps, for H-CHA, H-FAU, and H-MFI by ab initio methods.[20] Note that in H-CHA and H-FAU bridging hydroxyls with different local environments, and possibly different acidity, can coexist. H-SSZ-13 shows two different Brönsted acid sites, both with similar acidity, characterized by OH vibrational frequencies at 3616 and 3584 cm^{-1},[21] which were previously assigned to two different bridging oxygen atoms in the structure.[20,22] These are usually called high-frequency (HF) and low-frequency (LF) components, respectively, and are in the same range as the bridging hydroxyl in H-2dH (~3594 cm^{-1}). In the case of H-Y-Zeolite, also HF and LF IR bands are observed, located at ~3650 and ~3550 cm^{-1}, respectively.[23]

The rest of the Results and Discussion section will be organized as follows. Section 4.1 describes the thermal stability of bridging hydroxyls, which is important for future studies of catalytic activity. The experimental and theoretical results, for the interaction of bridging hydroxyls with weak bases, are described in Sections 4.2 and 4.3, respectively. Likewise, the interaction with strong bases is described in Sections 4.4 (experiment) and 4.5 (theory). In Section 4.6 we correlate the results from weak bases with the acidity in real zeolites. Finally, in Section 4.7 effects of adsorption energy and curvature are analyzed.

4.1. Thermal Stability of Bridging Hydroxyls. The thermal stability of bridging hydroxyls was examined by IRAS by monitoring the intensity of the OD vibration as a function of annealing temperature. This information will be vital for further studies of catalytic activity since it determines the range of temperatures at which the reactivity experiments can be carried out while still having bridging hydroxyls. Figure 2 shows the IR peak height at 2654 cm^{-1} (bridging OD) as a function of heating temperature for two different series (red circles and black squares). The original spectra from which the peak heights were measured are included in the Supporting Information. In all cases the IR spectrum was taken after letting the sample cool back down to 300 K. It is found that between 300 and 500 K there is a slight increase in the peak height, possibly due to a reorientation for the OD group, although care should be taken in this interpretation since the increase is almost within the experimental error. What is clear is that the intensity begins decreasing only at ~550 K, so that

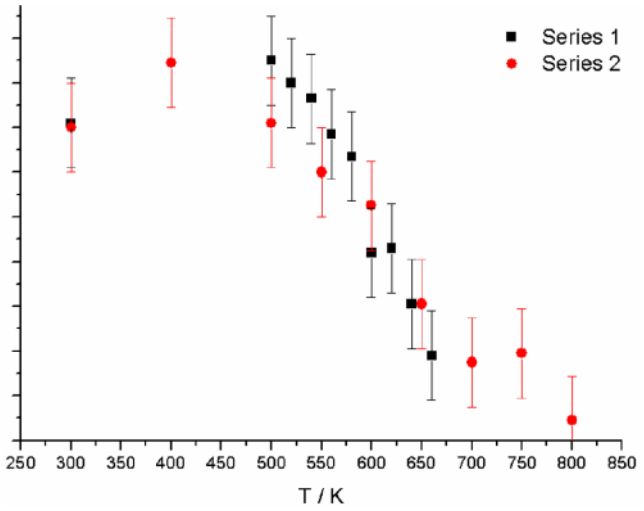

Figure 2. Plot of height of the IRAS peak corresponding to the vibration of bridging OD groups as a function of heating temperature for two different series.

mechanistic studies up to this temperature can be carried out using this film.

4.2. Weak Bases: Experimental Results. It is well-known for H-zeolites (and D-zeolites) that the weak bases CO and C_2H_4 form H-bonded complexes with acidic bridging hydroxyls. The interaction of these probe molecules with bridging hydroxyls is studied here for H-2dH and D-2dH.

Carbon Monoxide. The most widely used weak base to characterize bridging hydroxyls OH(br) on zeolites is CO. For H-2dH the latter induces a red-shift of the $\upsilon_{OH(br)}$ of 379 cm^{-1} (243 cm^{-1} for $\upsilon_{OD(br)}$), which is in the order of the most acidic OH(br) reported for zeolites. In parallel, the CO stretching vibration blue-shifts by 40 cm^{-1} with respect to the gas-phase CO molecule. Figure 3 shows a transmittance spectrum for CO adsorbed on a OD(br), divided by the spectrum taken before adsorption. This makes the absorption signal positive for the original OD stretching (2652 cm^{-1}), while the CO-coordinated OD group shows a negative signal for the OD (2409 cm^{-1}) and CO (2183 cm^{-1}) stretching modes.

Note that in IRAS, due to the selection rules, only modes with a component of the dynamic dipole moment normal to the surface can be observed. It is important to take this into account since this fact provides information about the geometry of the adsorbed molecules. Observing the 2183 cm^{-1} frequency indicates that the CO bond has a significant component perpendicular to the surface.

Ethene. Four spectra are shown in Figure 4, which will be described from top to bottom. The top one (a) corresponds to ethene dosed onto a nonhydroxylated surface. In this case, no peaks are observed in the spectrum, indicating the lack of ethene adsorption in the absence of bridging hydroxyls. The second spectrum (b) corresponds to a surface that has been hydroxylated with D_2O (D-2dH), showing frequencies corresponding to silanol groups (SiO–D) at 2763 cm^{-1} and bridging OD at 2655 cm^{-1}. The third spectrum (c) corresponds to a submonolayer amount of ethene adsorbed on the surface with deuterated hydroxyls. Ethene interacts with the bridging OD, through the π-electrons in the double bond, inducing a red-shift of 325 cm^{-1} (from 2655 to 2330 cm^{-1}). The last spectrum (d) corresponds to the saturation amount of ethene, resulting in the complete consumption of the 2655 cm^{-1} peak,

dx.doi.org/10.1021/jp405533s | J. Phys. Chem. C 2013, 117, 13547–13556

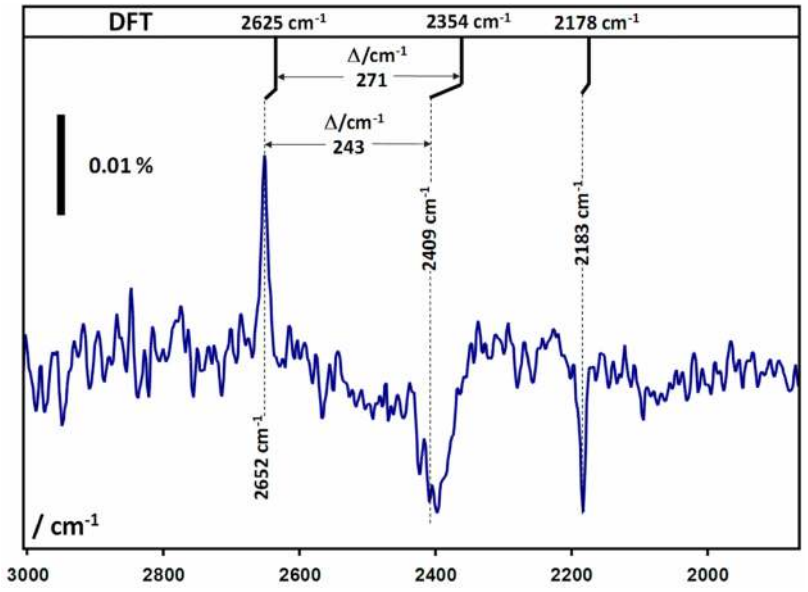

Figure 3. Transmittance spectrum of CO adsorbed on bridging OD groups divided by the spectrum taken before CO adsorption. Spectrum taken under CO pressure (2×10^{-5} mbar). At the top of the spectrum the DFT results are shown (double cell, Nachtigall[18] scheme, see Experimental section).

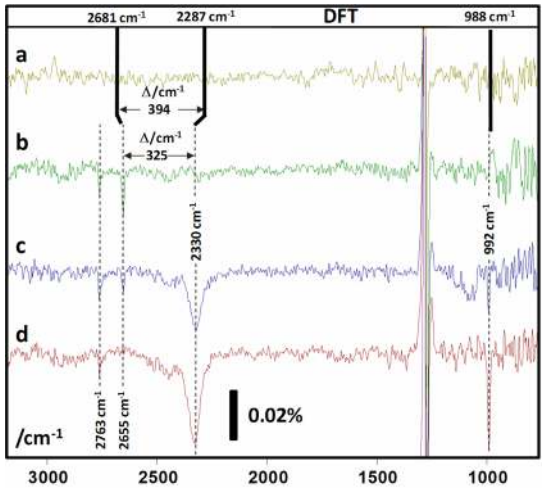

Figure 4. IRAS spectra of, from top to bottom, (a) ethene dosed on a film with no bridging hydroxyls, (b) a film with bridging OD groups before dosing ethene, and (c) and (d) after increasing doses of C_2H_4. At the top of the spectra the unscaled DFT frequencies are shown (double cell, unscaled harmonic frequencies, see Experimental section).

at the expense of the 2330 cm^{-1} peak. The only mode observed for ethene is the symmetric out-of-plane wagging of the H atoms. This indicates that the molecule plane is nearly parallel to the surface. Another indication of this geometry is the absence of the C═C stretching frequency in the spectra, which was previously shown to shift to lower frequencies upon interaction with acidic bridging hydroxyls.[16] Note that silanol groups (2763 cm^{-1}) do not interact with ethene. For the case of C_2H_4 on H-2dH, the shift is 487 cm^{-1} (from 3595 cm^{-1} to 3108 cm^{-1} (data not shown)).

The C_2H_4-perturbed bridging OD vibration (2330 cm^{-1}) appears significantly more intense and broader than the uncoordinated bridging OD (2655 cm^{-1}). Indeed, this behavior was previously reported in the literature for a study using a series of probe molecules on H-ZSM-5 where it was found that both the width of the IR peak and the intensity increase linearly with the basicity of the probe molecule, as measured by the induced shift.[24] This is a well-known effect in H-bonded species, and it can be explained by the increase in the O−H bond length which, in turn, results in an increase in the dipole moment and therefore also in its change upon stretching the bond.

Whereas Figures 3 and 4 report experiments on OD groups, Table 1 reports OH frequency shifts. The ν_{OD}/ν_{OH} ratio for the CO and C_2H_4 complexes, 0.749 and 0.750, respectively, deviates more from the ratio of the reduced masses for isolated (diatomic) OD/OH bonds (0.728) than for the free OD/OH bonds (0.738−0.739). Chakarova and Hadjiivanov[25] report similar results for H/D-ZSM-5, from which we get the ratios 0.738 for the free OH/D group and 0.745 for surface complexes with CO.

The reason for the deviation from the diatomic model is coupling of the OH/OD vibrations with other modes in the system. The free OH is energetically well separated from all other modes, and therefore coupling is negligible. The free OD group is significantly shifted to lower wavenumbers which will increase coupling with other modes due to a smaller energy difference. The largest effect is expected for OH/D bonds in the complexes because here the OH/D modes may couple in addition to intermolecular modes and their overtones. Thus, the observed deviations from the diatomic mass ratio in the complexes are in line with the observed line broadening.

We note that the ratio of the shifts f^{shift} given as

$$f^{shift} = f^{free} + (f^{free} - f^{complex}) \times \frac{\nu_{OH\text{-}complex}}{\Delta\nu_{OH}}$$

must not be expected to be close to the diatomic mass ratio because the OD/OH ratios are different for the free groups, f^{free}, and their counterparts in the complexes, $f^{complex}$. From our results we obtain 0.641 and 0.667 for the CO and C_2H_4 complexes, respectively, and the results for CO-H/D-ZSM-5[25] quoted above yield 0.661.

dx.doi.org/10.1021/jp405533s | J. Phys. Chem. C 2013, 117, 13547−13556

Table 1. Changes of OH Bond Distances, Δd_{OH} (in pm), As Well As Vibrational Frequencies, $\Delta\nu_{OH}$ (in cm^{-1}), for CO and C_2H_4 Adsorbed on the H-2dH Film Compared to Zeolites H-CHA and H-MFI

obsd		$\Delta\nu_{OH}$(CO)	$\Delta\nu_{CO}$		$\Delta\nu_{OH}(C_2H_4)$
H-MFI		−343. ± 8[a,c], −313 ± 3[c,d]			−389[b,c], −433 ± 8[c,d]
H-CHA		−316[e]	+34[e]		
H-2dH		−379	+40		−487
calcd	Δd_{OH}(CO)	$\Delta\nu_{OH}$(CO)[f]		$\Delta d_{OH}(C_2H_4)$	$\Delta\nu_{OH}(C_2H_4)$[g]
H-MFI					−535[h]
H-CHA	+2.66	−350	+48	+2.58	−537
H-2dH	+2.83	−373	+40	+2.63	−548

[a]Ref 28. [b]Ref 16. [c]Note that very broad bands are obtained which make it difficult to specify a precise number for the shift. [d]Ref 24. Taken from Figures 1 and 2 of that paper. [e]Ref 21 reports a shift of +39 cm^{-1}, but uses for CO the value of 2138 cm^{-1} (liquid like). Using our reference, 2143 cm^{-1}, for gas-phase CO, the shift is +34 cm^{-1}. [f]Anharmonic frequencies obtained from bond distances using the Nachtigall scheme.[18] [g]Unscaled harmonic frequencies [h]PBE calculations of Hansen et al.[29]

4.3. Weak Bases: Theoretical Results. Figure 5 compares the adsorption structures of CO and C_2H_4 on bridging hydroxyl groups on the 2dH film with those in H-chabasite. As expected from the missing C═C stretching mode in experimental IRAS spectra 4c and 4d, only a small tilt angle (12.7°) is found in the calculated structure for the vector defined by the C═C bond and the surface plane.

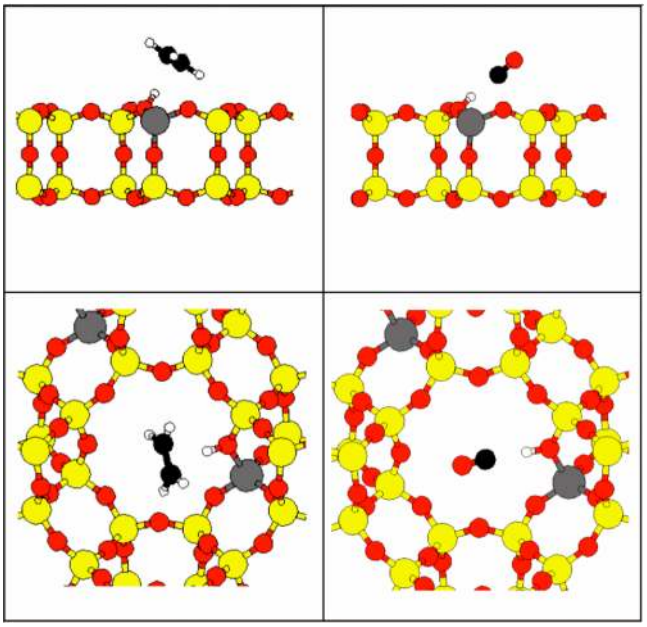

Figure 5. Adsorption structures of C_2H_4 (left) and CO (right) in H-2dH (top) and H-CHA (bottom).

Table 1 compares experimental and calculated OH frequency shifts on adsorption of CO and C_2H_4 on Brönsted sites of the 2dH film with zeolites H-CHA and H-ZSM-5. The ratio of the experimental shifts on C_2H_4 compared to CO adsorption is similar for H-MFI (1.38) and H-2dH (1.28). Comparing the 2dH films with the CHA and MFI zeolites, the experimental shifts are larger for the 2dH films indicating a higher acidity. The same is seen for the calculated vibrational frequencies. For both CO and C_2H_4 adsorption, the calculated shifts are larger for the 2dH film than for CHA (or MFI). It is important that this trend is reproduced, although for C_2H_4 adsorption the calculated shift numbers are too large. This is a well-known weakness of the exchange-correlation functional applied.[26] The OH bonds are too weak and too long, and on formation of a hydrogen bond they become too much elongated resulting in a too large red-shift. For CO adsorbed on bridging hydroxyls, it is possible to determine the CO and OH stretching frequencies directly from the corresponding DFT bond distances. This method proposed by Nachtigall[18] yields much improved vibrational frequencies as the required parameters have been found by comparison with high-level, i.e., CCSD(T), calculations.[18]

For the ethene complexes, where the frequency shifts are much larger, neither is it guaranteed that this correlation would work nor are the required parameters available. Here we use the unscaled harmonic frequencies. Scale factors, which would effectively account for too small harmonic force constants and neglected anharmonicities, are close to 1.0 for the PBE functional used anyway (a scale factor of 0.9948 yields a root-mean-square deviation of 38 cm^{-1}, see ref 27).

While Table 1 reports OH frequency shifts, Figures 3 and 4 report experiments on OD groups. A red-shift of 394 cm^{-1} was calculated for the O−D mode when adsorbing C_2H_4 (from 2681 to 2287 cm^{-1}) again larger than the 325 cm^{-1} shift observed experimentally (see top of Figure 4). Good agreement was found for the symmetric out-of-plane C−H wagging mode, yielding a frequency (988 cm^{-1}) close to the experimental value (992 cm^{-1}).

For CO on bridging OD, the results of the Nachtigall scheme for the OH frequencies have been multiplied with the ratio of the reduced masses, yielding a red-shift of 271 cm^{-1}, from 2625 to 2354 cm^{-1} for the O−D stretching vibration (see top of Figure 3).

4.4. Strong Bases: Experimental Results. When strong bases such as Py and NH_3 interact with the bridging hydroxyls of zeolites, it is a well-established fact that they abstract the proton to form PyH^+ and NH_4^+ ions, respectively. The interaction of these probe molecules with bridging hydroxyls will be studied here for H-2dH and D-2dH.

Pyridine (Py). The IR region between 1400 and 1700 cm^{-1} is usually analyzed to discern the state of the Py molecule in the adsorbed state. Four vibrational modes are commonly reported, designated 19b, 19a, 8b, and 8a, following the notation used in ref 30. For the coordinatively bound Py these modes are found at 1447−1460, 1488−1503, 1580, and 1600−1633 cm^{-1}, respectively.

When the molecule is protonated to form a pyridinium ion (PyH^+), these modes are observed at 1540, 1485−1500, 1620, and 1640 cm^{-1}. Figure 6 depicts the vibrational modes, along with the corresponding experimental frequencies, for a free Py molecule, as well as ranges of frequencies (see ref 30 and

dx.doi.org/10.1021/jp405533s | J. Phys. Chem. C 2013, 117, 13547−13556

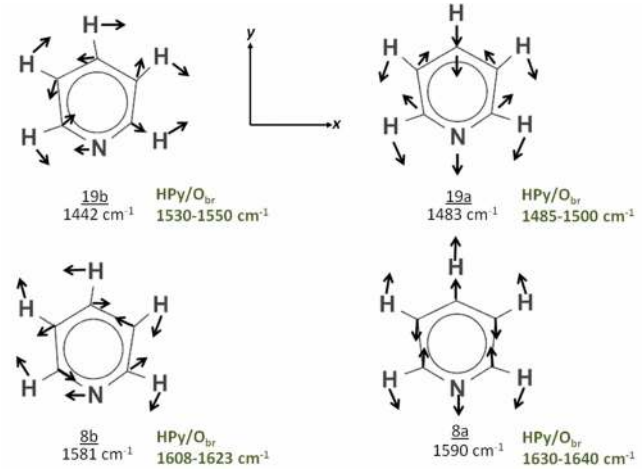

Figure 6. Pyridine modes between 1400 and 1700 cm^{-1}.

references therein) that have been reported for PyH^+ by adsorption on bridging hydroxyls. The most significant difference between Py and PyH^+ occurs in mode 19b, which undergoes a dramatic blue-shift of ~90 cm^{-1}.

In Figure 7, spectrum A corresponds to Py adsorbed at 300 K on a surface with no bridging hydroxyls. Two peaks are evident

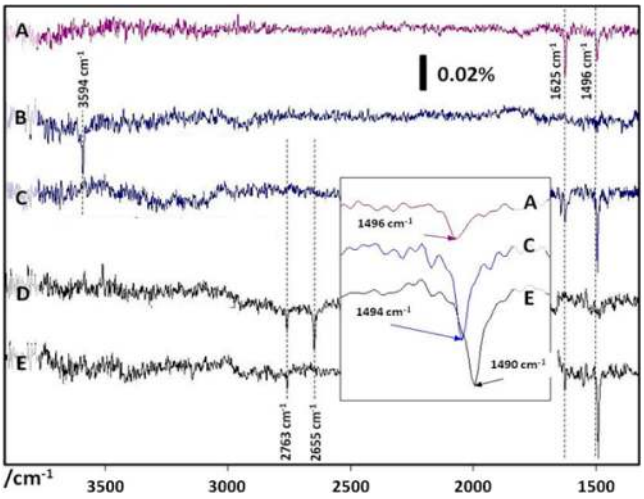

Figure 7. (A) Pyridine adsorbed on a nonhydroxylated surface. (B) Surface with bridging OH groups before and (C) after Py adsorption. (D) Surface with bridging OD groups before and (E) after pyridine adsorption. The inset shows mode 19a for the three different cases having Py on the surface.

at 1625 and 1496 cm^{-1}, which can be assigned to 8(a or b) and 19a of an adsorbed, nonprotonated Py. Since only vibrational modes that have a component perpendicular to the surface plane can be observed by IRAS, and considering the description of the modes shown in Figure 6, it is inferred that Py is adsorbed in an orientation such that the molecule plane has a significant component perpendicular to the surface plane, presumably with the N atom toward the surface. Spectrum B shows a surface that has been hydroxylated and shows a typical vibrational mode at 3594 cm^{-1}, corresponding to a bridging hydroxyl group. When Py is adsorbed on this surface (spectrum C), the O−H stretching peak disappears, and peaks corresponding to 8(a or b) and 19a modes appear in the spectrum at 1625 and 1494 cm^{-1}. The disappearance of the O−H vibration can be explained by the expected proton abstraction since its proton affinity (912 kJ/mol)[31] is higher than that of ammonia (854 kJ/mol), and it has been found previously by DFT that this is a nonactivated process.[30] Again, mode 19b, which usually allows a clear distinction between the protonated and nonprotonated forms, is not clearly observed in the spectrum due to the IRAS selection rules. The differences between the nonprotonated (A) and protonated (C) cases are subtle. They include a change in the intensities of the 19a and 8(a or b) modes, where 19a is more intense for the protonated case while 8(a or b) is significantly more intense for the nonprotonated one. Another difference is a 2 cm^{-1} red-shift in the 19a mode for the pyridinium ion with respect to the nonprotonated case. The same experiment was repeated for a bridging OD (spectrum D). Two peaks are observed in the O−D stretching region at 2763 and 2655 cm^{-1}, which correspond to a silanol group and a bridging OD group, respectively. (In spectrum B the silanol group is not observed since the spectrum that was used as a background already had silanol groups present). When pyridine is adsorbed on the surface with bridging OD groups (spectrum E), the peak at 2655 cm^{-1} disappears, indicating the deuteron abstraction by Py, while the silanol group remains. Again in this case, modes 19a and 8(a or b) are observed, but now mode 19a is shifted further down to 1490 cm^{-1}.

The fact that mode 19b is not observed leads to difficulties to clearly determine whether the molecule is protonated or not. However, this fact provides information about the orientation of the molecule. When defining the orientation of the molecule with respect to the surface plane two angles have to be considered. We are going to call them α and β, and these are depicted in Figure 8. α is the tilt of the molecule plane with

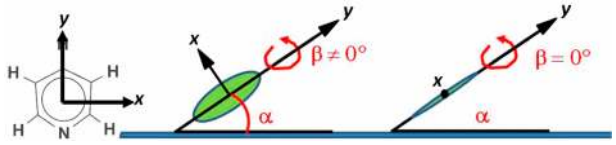

Figure 8. Green oval represents the pyridine molecule, and the angles $\boldsymbol{\alpha}$ and $\boldsymbol{\beta}$ define the orientation of the molecule with respect to the surface plane.

respect to the surface plane, while β is the rotation of the molecule around an axis defined along the N atom and the C atom in position 4 in the ring. Let us call this direction y, while x is the direction perpendicular to it within the plane of the molecule, as depicted in Figure 8. The main components of the 19b mode are in the x direction. The direction of the x axis depends on the angle β, and it becomes parallel to the surface with $\beta = 0$. Since only modes perpendicular to the surface can be seen by IRAS, this means that for the mode 19b not to be observed β must be ~0. In addition, for mode 19a to be observed, α must be >0.

Ammonia. Ammonia is another frequently used probe molecule in the characterization of zeolites.

Figure 9 shows a spectrum obtained after adsorption of NH_3 on a surface with bridging hydroxyls, using as a background a spectrum taken before the adsorption of the molecule. The mode associated with the bridging hydroxyl O−H stretching (3598 cm^{-1}) shows a positive intensity, indicating that the adsorption of NH_3 resulted in either the proton abstraction or

dx.doi.org/10.1021/jp405533s | J. Phys. Chem. C 2013, 117, 13547−13556

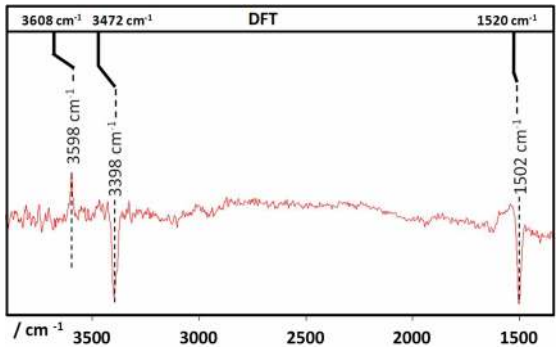

Figure 9. Spectrum of ammonia adsorbed on a bridging hydroxyl using as a background the spectrum taken before adsorption. At the top of the spectra DFT frequencies are shown. The unscaled values are shown for the umbrella and NH stretching mode, whereas the 3608 cm^{-1} for the OH stretching mode is the result of the Nachtigall scheme. The calculations were done using a double cell (see Experimental section).

shift to lower frequency. Two other peaks appear in the spectrum, located at 3398 and 1502 cm^{-1}.

4.5. Strong Bases: Theoretical Results. Figure 10 shows the adsorption structures of NH_3 and pyridine obtained by DFT.

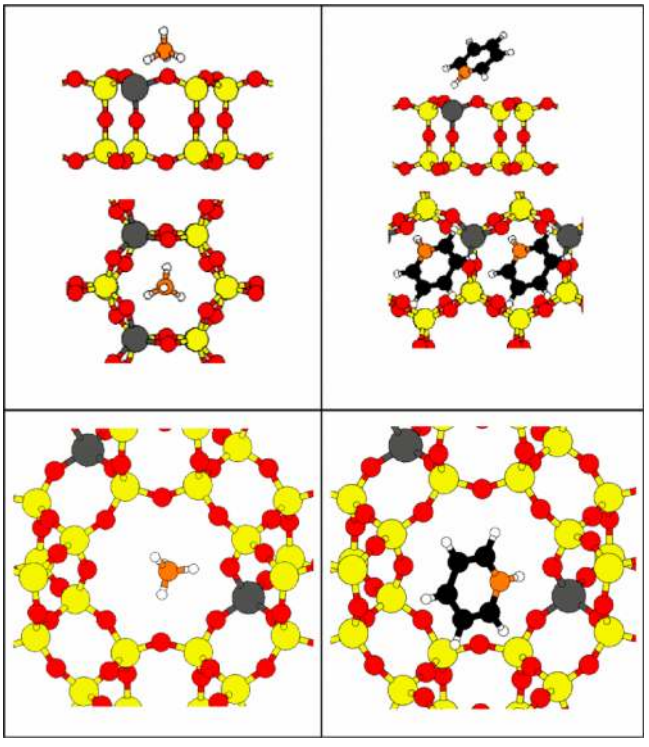

Figure 10. Adsorption structures of NH_3 (left) and pyridine (right) on H-2dH (top) and H-CHA (bottom).

Pyridine. There is good agreement of the DFT structure (Figure 10) with the experimental results in terms of the molecular orientation; the calculated value for α is 34°, and the one for β is 12°. In these calculations, mode 19a has a frequency of 1470 cm^{-1} for the bridging OH, while it is 1462 cm^{-1} for the bridging OD. This shift to lower frequencies for mode 19a, when comparing the protonated to the deuterated case, is in agreement with what is found experimentally.

Ammonia. Figure 10 shows that a protonated structure has formed, with the ammonium ion located on top of the center of the six-membered ring and three of the H atoms pointing toward the surface forming H-bonds to three of the O atoms of the ring, two of which are part of the AlO_4 tetrahedron.

There are two vibrational modes of NH_4^+ with strong components perpendicular to the surface plane in this configuration, which are present in the regions where the experimental modes are found. These are a N−H stretch for the H pointing outward from the surface (3472 cm^{-1}) and an umbrella mode also perpendicular to the surface plane at 1520 cm^{-1}. This allows the assignment of the two modes observed experimentally (Figure 9), in agreement with hypothesis of the proton abstraction, which is expected based on what is known from bulk zeolites. Other modes of lower intensity can be expected for protonated ammonia, such as the small feature at 1680 cm^{-1},[32] although the intensity is too close to the noise level and we prefer not to discuss it here. The DFT O−H frequency for the unloaded zeolite is found at 3608 cm^{-1}, whereas the Nachtigall scheme was used for the latter value; the former two are unscaled harmonic frequencies, all calculated for a double cell.

4.6. Acidity of Bridging Hydroxyls. The measurement of solid acidity by using probe molecules has been controversially discussed, especially when trying to establish a comparison with the more familiar concept of acidity in solution.[7] Umansky et al. compared the acidity in solids with the concept of Hammett acidity by using a spectrophotometric method involving indicators that change color depending on the acidity of the site and compared the results with sulfuric acid solutions using the same indicators.[33] Lavalley later took these results and correlated them with the acidity obtained using the probe molecules CO and C_2H_4.[15]

In Sections 4.2 and 4.3 we described the cases of CO and C_2H_4 interacting with H-2dH and D-2dH. Since there is a strong dependence of the catalytic activity of zeolites with the acidity of the bridging hydroxyl,[15,33] it is useful to analyze, in further detail, the shifts in H-2dH induced by weak bases and compare with data available in the literature for hydroxyls in other materials, with particular emphasis on bridging hydroxyls in zeolites and related materials. Table 2 shows a list of materials with a well-defined structure and the shifts induced by CO and C_2H_4. These data points are plotted in Figure 11, where the *x*- and *y*-axis correspond to the C_2H_4 and CO induced shifts, respectively. A more extensive version of this table and the corresponding figures are included in the Supporting Information, including cases for which the structure is not well-defined and other cases in which only one of these probe molecules was used. There is a clear correlation between the shifts induced by C_2H_4 and CO, as it had already been noticed by Lavalley et al.[15] The trend is extensive also to other materials, and it seems to be independent of the type of hydroxyl group, as is seen in the figure in the Supporting Information. For clarity, we will concentrate our attention on systems with well-defined structure. However, it should be noted that some dealumination processes result in materials with higher acidity than the ones described here but for which the structure of the active site is not well-established.

The black squares in Figure 11 correspond to the same H−Y zeolite (FAU framework). **Y0** is a nondealuminated H−Y zeolite. **Y1** was dealuminated by isomorphous substitution by treatment with $(NH_4)_2SiF_6$. The blue star corresponds to H-ZSM-5 (MFI framework type).[24] The red triangles correspond

dx.doi.org/10.1021/jp405533s | J. Phys. Chem. C 2013, 117, 13547−13556

Table 2. Magnitude of the Shifts in OH Vibrations Reported in the Literature and in This Work for Different Materials upon Adsorption of CO and C_2H_4 (These are Shown Graphically in the Plot in Figure 11)

Δν(OH)/cm^{-1}		Material (see Ref.	Framework	Ref.	Symbol
CO	C_2H_4	for details)	Type		
379	**487**	**H-2dH**	***NA***	**This work**	**●(H)**
373	**548**	**DFT H-2dH**	***NA***	**This work**	**▲ (H*)**
316		H-SSZ-13	CHA	[21]	●●●●(C)
350	**537**	**DFT H-CHA**	**CHA**	**This work**	**▲ (C*)**
278	274	H-SAPO-34	CHA	[34]	▼(S)
332	449	H-SAPO-34	CHA	[34]	▼(S)
155	250	H-SAPO-34	CHA	[34]	▼(S)
172	285	H-Y[a]	FAU	[35]	■(Y1)
299	405	H-Y	FAU	[35]	■(Y0)
298	431	H-Y[a]	FAU	[35]	■(Y1)
313±3[b]	433±8[b]	H-ZSM-5	MFI	[24]	★(Z)

[a]Dealuminated by isomorphous substitution. [b]Ref 24. Taken from Figures 1 and 2 of that paper.

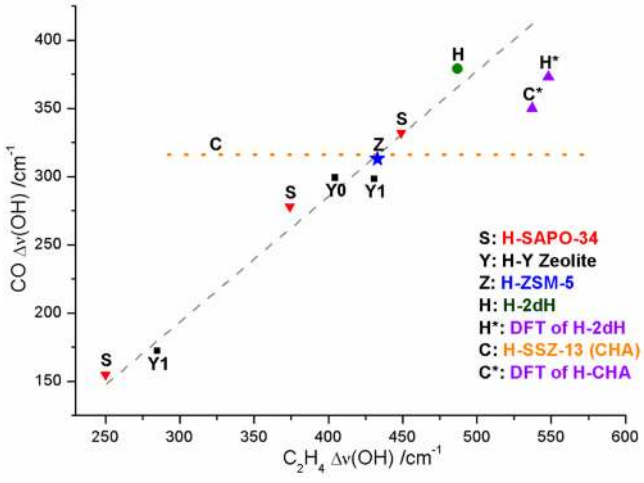

Figure 11. Plot of C_2H_4 (*x*-axis) and CO (*y*-axis) induced shifts in the OH vibration for a variety of samples, including the film reported in this work (green circle).

to H-SAPO-34, a silicoaluminophosphate with CHA structure.[34] The orange dotted line corresponds to H-SSZ-13, a zeolite with CHA framework. The red-shifts induced by C_2H_4 and CO adsorption on bridging OH groups of H-2dH are 487 and 379 cm^{-1}, respectively (shown by a green circle with the label **H**). The DFT calculations from this work are also included in the plot (purple triangle), labeled **C*** for the H-CHA framework and **H*** for H-2dH. Note however that for the results from DFT calculations the frequencies were calculated by different methods for CO (Nachtigall scheme) and C_2H_4 (unscaled frequencies), which accounts for the deviation of these points from the experimental trend in terms of absolute values. Nevertheless, the general trend is reproduced by the calculations, in terms of that the bridging hydroxyls in H-2dH are the most acidic when compared to other zeolites. This high acidity should result in a strong catalytic activity (reactivity studies are on the way).[15] As mentioned above, Umansky et al. showed correlations between the acidity of the OH groups and their catalytic activity toward the conversion of isobutene, indicating that more acidic hydroxyls are more active toward cracking of the molecule.[33]

For H-2dH we have identified only one type of bridging OH group, with the proton pointing toward what can be thought of as an infinitely large cavity. For simplicity here we will consider that the distribution of nearest neighbor (NN) Al atoms does not have an influence on the vibrational frequency and the acidity of the site. In fact, in our previous report, DFT calculations showed differences of only 2 cm^{-1} between the two sites with different NN distributions considered in that case.[8] For the case of H-SSZ-13 (H-CHA framework) there are four structurally different oxygen atoms. Bordiga et al.[21] determined that the low-frequency (3584 cm^{-1}) band corresponds to the least accessible O-atom (O3), which is the only one that does not form part of an eight-membered ring in the structure, and the high-frequency band (3616 cm^{-1}) is a result of contributions of the remaining three positions (O1, O2, and O4). All sites seem to have similar acidic strength, as measured by a CO induced shift of 316 cm^{-1} (orange horizontal dotted line in Figure 11),[21] which is lower than the shift for H-2dH (379 cm^{-1}). While only one cavity size is present in the CHA framework (cha cage), the FAU framework counts with two different cavities, i.e., small sodalite (or *β*-) and large supercages. IR[36] and neutron diffraction[37] studies determined that the two peaks observed in the bridging OH region for HY zeolites correspond to OH groups pointing toward the two cages, with the high-frequency band (3650 cm^{-1}) from the supercage and the low-frequency band (3550 cm^{-1}) from the *β*-cage. For nondealuminated HY, only the acidity of the high-frequency band can be probed with CO, for which induced

dx.doi.org/10.1021/jp405533s | J. Phys. Chem. C 2013, 117, 13547−13556

Table 3. PBE+D Adsorption Energies (Dispersion Contribution in Parentheses) of CO, C_2H_4, NH_3, and NC_5H_5 on Zeolite H-CHA and on the H-2dH Film (in kJ/mol)[a]

system	M:cell[b]	CO	C_2H_4	NH_3	NC_5H_5
H-CHA	1:2	40.4 (19.3)	53.3 (36.8)	158.6(27.4)	182.2 (66.4)
H-2dH	1:2	37.8 (15.2)	48.4 (25.5)	160.2 (28.8)	145.1 (47.1)
difference		2.6 (4.1)	4.9 (11.3)	−1.6 (−1.4)	37.1 (19.3)
H-2dH	2:2	37.8 (15.1)	49.1 (27.4)	155.1(29.0)	132.6 (54.8)
$\Delta E_{lateral}$[c]		0.0	−0.7	+5.0	+12.5

[a]The gas-phase molecule was calculated using the same cell parameters as in the adsorbed structure. [b]Loading, number of molecules per (OH group = cells). [c]Lateral interaction energy $\Delta E_{lat.} = \Delta E_{ads}$ (1:2) − ΔE_{ads} (2:2); positive numbers indicate repulsion.

shifts of 299 cm^{-1} for H−Y[35] (see point **Y0** in Figure 11) and 288 cm^{-1} for (H, Na)-Y[23] were reported. These values are in the same range as the H-SSZ-13 case. However, upon dealumination of H−Y by isomorphous substitution (**Y1**) the bridging OH in the β-cage becomes accessible to CO molecules. This is the **Y1** point with smaller ν_{OH} shifts.

4.7. Adsorption Energies and Surface Curvature Effects. Table 3 shows the adsorption energies, which are defined as positive numbers according to

$$\Delta E_{ads} = E_{ads}(\text{H-Z}) + E(\text{M}) - E_{ads}(\text{M/H-Z})$$

Experimental results are hardly available. Hansen et al.[29] quote a value of 40.5 kJ/mol which they derived from experimental heat of adsorption on a (H,Na)-zeolite Y[38] and vibrational corrections as well as thermal corrections form DFT +D calculations. They performed hybrid MP2:PBE+D + ΔCCSD(T) calculations for C_2H_4/H-MFI and obtained an adsorption energy of 48.3 kJ/mol.[29]

For CO and C_2H_4, the calculated adsorption energies are 2.6 and 4.9 kJ/mol, respectively, smaller on the flat surfaces of the film than in the cavities of chabasite. This illustrates the effect of missing pore fit which has been observed before (see ref 11 and references therein), when comparing adsorption in small (better fit) and large pores (less good fit). The increase from the flat surface to the cavity is even more pronounced when looking at the dispersion contribution only: 4.1 and 11.3 kJ/mol for CO and C_2H_4. That the effect is larger for the dispersion contribution than for the total adsorption energy implies that there must be another component, which is stronger for the 2dH film than for chabasite. This is nothing else than the specific interaction governed by acidity that we found to be stronger for the 2dH film than for chabasite in previous sections.

5. CONCLUSIONS

The interaction of bases of different strength with bridging hydroxyls was studied on a zeolite model system (H-2dH) with a well-defined structure under the controlled conditions provided by a UHV environment. While ammonia and pyridine abstract the proton from the bridging hydroxyl to form ammonium and pyridinium ions, respectively, weak bases CO and C_2H_4 bind coordinatively to the proton inducing a shift in the O−H vibration. This shift is proportional to the acidity of the site and indicates that the aluminosilicate film is more acidic than conventional zeolites with cavities. However, the adsorption energies are larger in cavities because of larger dispersion contributions for curved surfaces.

An acidity in the range of the most acidic (and catalytically active) zeolites validates the use of this well-defined aluminosilicate film as a model system for mechanistic studies of the large number of chemical reactions that are performed on zeolites and paves the way for improvements in the currently used industrial catalysts once the mechanistic details are well understood. In particular, C_2H_4 constitutes an important case since the formation of the bridging OH−C_2H_4 adduct reported here is the first step in the ethene oligomerization process catalyzed by bridging hydroxyls. Additionally, the internal vibrational modes of the probe molecules allowed us to infer their orientation with respect to the bridging hydroxyl taking advantage of the IRAS selection rules.

■ ASSOCIATED CONTENT

Supporting Information

Coordinates of the atoms for the minimum energy structures calculated by DFT are included as well as the experimental data taken to characterize the film before the study with probe molecules. These data include STM images, XP spectra, LEED image, and IRA spectra of phonon vibrations. The IRA spectra as a function of heating temperature used to prepared Figure 2 as well as more extensive versions of Table 2 and Figure 11 are also included. In addition, tables with the calculated frequencies for the different vibrational modes are included for all the probe molecules interacting with the hydroxyls of 2dH and CHA, along with the OH (OD) bond distances with and without the probe molecule adsorbed. A table with ν(OD)/ν(OH) ratios and the original frequencies from which they were obtained is also included. This material is available free of charge via the Internet at http://pubs.acs.org.

■ AUTHOR INFORMATION

Corresponding Author

*J. Anibal Boscoboinik. Phone: +49 30 8413 4218. E-mail address: bosco@fhi-berlin.mpg.de. Joachim Sauer. Phone: +49 30 2093 7135. E-mail address: js@chemie.hu-berlin.de.

Notes

The authors declare no competing financial interest.

■ ACKNOWLEDGMENTS

This work has been supported by the German Science Foundation (DFG) by a computer grant from the North German Computing Alliance Berlin − Hannover (HLRN) and by the Funds of the Chemical Industry. J.A. Boscoboinik gratefully acknowledges a fellowship by the Alexander von Humboldt Foundation, and F. Fischer gratefully acknowledges a Kekule scholarship by the Funds of the Chemical Industry. F. Fischer also thanks R. Wlodarczyk (Berlin) for helpful discussions.

REFERENCES

(1) Lin, C. C. H.; Dambrowitz, K. A.; Kuznicki, S. M. Evolving Applications of Zeolite Molecular Sieves. *Can. J. Chem. Eng.* **2012**, *90*, 207−216.

(2) Yilmaz, B.; Müller, U. Catalytic Applications of Zeolites in Chemical Industry. *Top. Catal.* **2009**, *52*, 888−895.

(3) Lamberti, C.; Zecchina, A.; Groppo, E.; Bordiga, S. Probing the Surfaces of Heterogeneous Catalysts by in Situ IR Spectroscopy. *Chem. Soc. Rev.* **2010**, *39*, 4951−5001.

(4) Sauer, J.; Eichler, U.; Meier, U.; Schäfer, A.; von Arnim, M.; Ahlrichs, R. Absolute Acidities and Site Specific Properties of Zeolite Catalysts Modelled by Advanced Computational Chemistry Technology. *Chem. Phys. Lett.* **1999**, *308*, 147−154.

(5) Sauer, J.; Sierka, M. Combining Quantum Mechanics and Interatomic Potential Functions Inab Initio Studies of Extended Systems. *J. Comput. Chem.* **2000**, *21*, 1470−1493.

(6) Freund, H. J. Model Studies in Heterogeneous Catalysis. *Chem.—Eur. J.* **2010**, *16*, 9384−9397.

(7) Haw, J. F. Zeolite Acid Strength and Reaction Mechanisms in Catalysis. *Phys. Chem. Chem. Phys.* **2002**, *4*, 5431−5441.

(8) Boscoboinik, J. A.; Yu, X.; Yang, B.; Fischer, F. D.; Włodarczyk, R.; Sierka, M.; Shaikhutdinov, S.; Sauer, J.; Freund, H.-J. Modeling Zeolites with Metal-Supported Two-Dimensional Aluminosilicate Films. *Angew. Chem., Int. Ed.* **2012**, *51*, 6005−6008.

(9) Boscoboinik, J. A.; Yu, X.; Yang, B.; Shaikhutdinov, S.; Freund, H.-J. Building Blocks of Zeolites on an Aluminosilicate Ultra-Thin Film. *Microporous Mesoporous Mater.* **2013**, *165*, 158−162.

(10) Lercher, J. A.; Gründling, C.; Eder-Mirth, G. Infrared Studies of the Surface Acidity of Oxides and Zeolites Using Adsorbed Probe Molecules. *Catal. Today* **1996**, *27*, 353−376.

(11) Lucas, A. A.; Derycke, I.; Lambin, P.; Vigneron, J. P.; Leherte, L.; Elanany, M.; André, J. M.; Larin, A. V.; Vercauteren, D. P. Confinement in Molecular Sieves: The Pioneering Physical Concepts. *J. Mol. Catal. A: Chem.* **2009**, *305*, 16−23.

(12) Nicholas, J. B.; Haw, J. F. The Prediction of Persistent Carbenium Ions in Zeolites. *J. Am. Chem. Soc.* **1998**, *120*, 11804−11805.

(13) Termath, V.; Haase, F.; Sauer, J.; Hutter, J.; Parrinello, M. Understanding the Nature of Water Bound to Solid Acid Surfaces. Ab Initio Simulation on HSAPO-34. *J. Am. Chem. Soc.* **1998**, *120*, 8512−8516.

(14) Sauer, J. Proton Transfer in Zeolites. In *Hydrogen-Transfer Reactions*; Hynes, J. T., Klinman, J. P., Limbach, H.-H., Schowen, R. L., Eds.; Wiley-VCH: Weinheim, 2007; pp 685−707.

(15) Lavalley, J.-C.; Jolly-Feaugas, S.; Janin, A. Saussey, In Situ Fourier Transform Infrared Studies of Active Sites and Reaction Mechanisms in Heterogeneous Catalysis: Hydrocarbon Conversion on H-Zeolites. *Mikrochim. Acta, Suppl.* **1997**, *14*, 51−56.

(16) Spoto, G.; Bordiga, S.; Ricchiardi, G.; Scarano, D.; Zecchina, A.; Borello, E. IR Study of Ethene and Propene Oligomerization on H-ZSM-5: Hydrogen-Bonded Precursor Formation, Initiation and Propagation Mechanisms and Structure of the Entrapped Oligomers. *J. Chem. Soc., Faraday Trans.* **1994**, *90*, 2827−2835.

(17) Martínez, C.; Corma, A. Inorganic Molecular Sieves: Preparation, Modification and Industrial Application in Catalytic Processes. *Coord. Chem. Rev.* **2011**, *255*, 1558−1580.

(18) Nachtigall, P.; Bludsky, O.; Grajciar, L.; Nachtigallova, D.; Delgado, M. R.; Arean, C. O. Computational and FTIR Spectroscopic Studies on Carbon Monoxide and Dinitrogen Adsorption on a High-Silica H-FER Zeolite. *Phys. Chem. Chem. Phys.* **2009**, *11*, 791−802.

(19) Baerlocher, C.; McCusker, L. B. *Database of Zeolite Structures*: http://www.iza-structure.org/databases/ (accessed 01/05/2013).

(20) Sierka, M.; Sauer, J. Proton Mobility in Chabazite, Faujasite, and ZSM-5 Zeolite Catalysts. Comparison Based on ab Initio Calculations. *J. Phys. Chem. B* **2001**, *105*, 1603−1613.

(21) Bordiga, S.; Regli, L.; Cocina, D.; Lamberti, C.; Bjørgen, M.; Lillerud, K. P. Assessing the Acidity of High Silica Chabazite H-SSZ-13 by FTIR Using CO as Molecular Probe: Comparison with H-SAPO-34. *J. Phys. Chem. B* **2005**, *109*, 2779−2784.

(22) Smith, L. J.; Davidson, A.; Cheetham, A. K. A Neutron Diffraction and Infrared Spectroscopy Study of the Acid Form of the Aluminosilicate Zeolite, Chabazite (H-SSZ-13). *Catal. Lett.* **1997**, *49*, 143−146.

(23) Gribov, E. N.; Cocina, D.; Spoto, G.; Bordiga, S.; Ricchiardi, G.; Zecchina, A. Vibrational and Thermodynamic Properties of Ar, N2, O2, H2 and CO Adsorbed and Condensed Into (H,Na)-Y Zeolite Cages As Studied by Variable Temperature IR Spectroscopy. *Phys. Chem. Chem. Phys.* **2006**, *8*, 1186−1196.

(24) Makarova, M. A.; Ojo, A. F.; Karim, K.; Hunger, M.; Dwyer, J. FTIR Study of Weak Hydrogen Bonding of Broensted Hydroxyls in Zeolites and Aluminophosphates. *J. Phys. Chem.* **1994**, *98*, 3619−3623.

(25) Chakarova, K.; Hadjiivanov, K. H-Bonding of Zeolite Hydroxyls with Weak Bases: FTIR Study of CO and N2 Adsorption on H-D-ZSM-5. *J. Phys. Chem. C* **2011**, *115*, 4806−4817.

(26) Sauer, J.; Ugliengo, P.; Garrone, E.; Saunders, V. R. Theoretical Study of van der Waals Complexes at Surface Sites in Comparison with the Experiment. *Chem. Rev.* **1994**, *94*, 2095−2160.

(27) Merrick, J. P.; Moran, D.; Radom, L. An Evaluation of Harmonic Vibrational Frequency Scale Factors. *J. Phys. Chem. A* **2007**, *111*, 11683−11700.

(28) Zecchina, A.; Bordiga, S.; Spoto, G.; Scarano, D.; Petrini, G.; Leofanti, G.; Padovan, M.; Areàn, C. O. Low-Temperature Fourier-Transform Infrared Investigation of the Interaction of CO with Nanosized ZSM5 and Silicalite. *J. Chem. Soc., Faraday Trans.* **1992**, *88*, 2959−2969.

(29) Hansen, N.; Kerber, T.; Sauer, J.; Bell, A. T.; Keil, F. J. Quantum Chemical Modeling of Benzene Ethylation over H-ZSM-5 Approaching Chemical Accuracy: A Hybrid MP2:DFT Study. *J. Am. Chem. Soc.* **2010**, *132*, 11525−11538.

(30) Castellà-Ventura, M.; Akacem, Y.; Kassab, E. Vibrational Analysis of Pyridine Adsorption on the Brønsted Acid Sites of Zeolites Based on Density Functional Cluster Calculations. *J. Phys. Chem. C* **2008**, *112*, 19045−19054.

(31) Busca, G. The Surface Acidity of Solid Oxides and Its Characterization by IR Spectroscopic Methods. An Attempt at Systematization. *Phys. Chem. Chem. Phys.* **1999**, *1*, 723−736.

(32) Zecchina, A.; Marchese, L.; Bordiga, S.; Pazè, C.; Gianotti, E. Vibrational Spectroscopy of NH4+ Ions in Zeolitic Materials: An IR Study. *J. Phys. Chem. B* **1997**, *101*, 10128−10135.

(33) Umansky, B.; Engelhardt, J.; Hall, W. K. On the Strength of Solid Acids. *J. Catal.* **1991**, *127*, 128−140.

(34) Martins, G. A. V.; Berlier, G.; Coluccia, S.; Pastore, H. O.; Superti, G. B.; Gatti, G.; Marchese, L. Revisiting the Nature of the Acidity in Chabazite-Related Silicoaluminophosphates: Combined FTIR and 29Si MAS NMR Study. *J. Phys. Chem. C* **2007**, *111*, 330−339.

(35) Maache, M., Etude par spectroscopie infrarouge de l'effet de la structure et de la désalumination de divers zéolithes sur leur acidité de Bronsted. *Ph.D. Thesis*. Université de Caen, Caen, France, 1992.

(36) Anderson, M. W.; Klinowski, J. Zeolites Treated with Silicon Tetrachloride Vapour. IV. Acidity. *Zeolites* **1986**, *6*, 455−466.

(37) Czjzek, M.; Jobic, H.; Fitch, A. N.; Vogt, T. Direct Determination of Proton Positions in D-Y and H-Y Zeolite Samples by Neutron Powder Diffraction. *J. Phys. Chem.* **1992**, *96*, 1535−1540.

(38) Cant, N. W.; Hall, W. K. Studies of the Hydrogen Held by Solids: XXI. The Interaction between Ethylene and Hydroxyl Groups of a Y-Zeolite at Elevated Temperatures. *J. Catal.* **1972**, *25*, 161−172.